OPEN ACCESS
IOP Publishing | ISECAEP
Journal of Reliability Science and Engineering
J. Reliab. Sci. Eng. **2** (2026) 025101 (16pp)
https://doi.org/10.1088/3050-2454/ae524d

Assessment of time-variant reliability of high-temperature rotating structure by CD-DT interference incorporating adaptive surrogate model

Hang-Hang Gu[1], Yuan-Ze Tang[1], Xinyu Yang[2], Run-Zi Wang[3,4,*] and Xian-Cheng Zhang[1]

[1] Key Laboratory of Pressure Systems and Safety, Ministry of Education, East China University of Science and Technology, Shanghai 200237, People's Republic of China
[2] Institute of High Performance Computing (IHPC), Agency for Science, Technology and Research (A∗STAR), 1 Fusionopolis Way, #16-16 Connexis, Singapore 138632, Singapore
[3] Advanced Institute for Materials Research (WPI-AIMR), Tohoku University, Sendai 9808577, Japan
[4] Department of Materials Processing, Graduate School of Engineering, Tohoku University, Sendai 9808579, Japan

E-mail: runzi.wang.a7@tohoku.ac.jp

Received 30 December 2025, revised 28 February 2026
Accepted for publication 15 March 2026
Published 31 March 2026

Abstract

High-temperature rotating structures (HTRSs) are essential components in industries, operating under severe conditions that lead to unpredictable failure behaviors. These failures are driven by uncertainties in material properties, loading conditions, and geometric variations. This study proposes a robust computational framework for assessing probabilistic damage accumulations (PDAs) and system-level reliability of HTRS under multi-source uncertainties. The probabilistic properties of basic random variables (RVs) in spatial and temporal scale are accounted, which are used to analyze PDA across different scenarios and reliability is assessed using the cumulative damage–damage threshold interference criterion. An adaptive surrogate model is then developed to approximate the complex, nonlinear relationship between damage and RVs, ensuring efficient and accurate simulations. Numerical case studies demonstrate the high efficiency and precision of the proposed method, which is further applied to a turbine disk considering multi-source uncertainties. The proposed method significantly improves computational efficiency while maintaining high accuracy in predicting system reliability, providing new insights in the damage-driven reliability assessment upward to system-level applications.

Keywords: probabilistic damage accumulation, CD-DT criterion, adaptive surrogate model, reliability assessment

* Author to whom any correspondence should be addressed.

Original content from this work may be used under the terms of the Creative Commons Attribution 4.0 licence. Any further distribution of this work must maintain attribution to the author(s) and the title of the work, journal citation and DOI.

© 2026 The Author(s). Published by IOP Publishing Ltd on behalf of the Institute of Systems Engineering, China Academy of Engineering Physics

1. Introduction

High-temperature rotating structures (HTRSs) are critical components in modern process industries, playing essential roles in aerospace, power generation, and chemical processing applications [1–4]. As the demand for energy efficiency increases, the operational conditions of these structures have become more severe and complex [5, 6]. For example, in the quest to improve the thrust-to-weight ratio in aircraft engines, turbine inlet temperatures and rotational speeds have reached unprecedented levels [7]. While these technological advances are crucial for meeting the rising performance demands of aeroengines, they also introduce significant challenges related to material strength and structural integrity. In particular, the high temperatures and extreme centrifugal forces lead to gradual material degradation, increasing the likelihood of unpredictable failures. HTRSs are subjected to multiple sources of uncertainty, including the variations in material properties [8], manufacturing variations [9, 10] and operational conditions [11]. These uncertainties contribute to stochastic failure behaviors, making it difficult to ensure the reliability and safety of critical components. Therefore, evaluating the reliability of HTRSs throughout their designed lifespan is of paramount importance.

Over the past few decades, the stress-strength interference criterion has been used to address reliability assessment challenges in engineering [12–14]. It treats stress and strength as random variables (RVs), with the overlap of their distributions representing the probability of failure. Previous studies have demonstrated the effectiveness of this criterion in the static structures like bridges and pressure vessels, where loading conditions are relatively constant over time [15, 16]. For instance, Fang *et al* [17] developed a structural reliability prediction model using stress-strength interference, while Nadarajah *et al* [18] extended the criterion to account for bivariate distribution dependencies. However, applying this criterion to HTRSs is far more complex due to their exposure to extreme operational conditions, such as cyclic loading and elevated temperatures [19, 20]. Specifically, the intrinsic strength of components diminishes over time due to fatigue effects, which are exacerbated by the cyclic stresses they experience during operation [21–25]. The reliability of HTRSs is inherently time-variant, influenced by the gradual degradation of material strength under cyclic stresses [26]. In response to this challenge, researchers have developed the cyclic stress-residual strength interference criterion to incorporate the effects of cyclic loading on residual strength, providing a more accurate failure probability estimation over time [27–30]. Notable examples include Schaff and Davidson [31] and Yao and Himmel [32], who proposed deterministic residual strength models to capture the degradation process. Further advancements by Gao and An [33] used Weibull distributions to model residual strength under constant amplitude cyclic loading. Despite the theoretical promise of these criteria, experimental validation remains costly and complex, as modeling the strength degradation process under uncertainty is extremely challenging.

Given these limitations, residual strength may not always be appropriate for modeling HTRS degradation under complex cyclic loading. In recent years, damage-based reliability frameworks have gained prominence for their ability to integrate physics-based degradation models with probabilistic analysis [34–36]. For instance, Kong *et al* [37] proposed a fatigue damage accumulation model for a high-pressure oil pipe based on fatigue probability, using a log-normal distribution to describe fatigue life dispersion and introducing a load-level-dependent interaction factor to account for damage equivalence between different stress levels. Peng *et al* [38] further developed a probabilistic double linear damage rule, which explicitly separates the fatigue process into crack initiation and propagation stages. By assuming normal distribution for fatigue life and employing a one-to-one probability density function transformation, the model derives time-dependent statistical moments for cumulative damage and damage threshold (CD-DT), enabling time-variant reliability assessment under both constant and variable amplitude loading. Recently, Gu *et al* [39] developed a damage-driven reliability assessment framework for HTRS such as steam turbine rotors. This framework integrates probabilistic damage analysis, weak-site correlation analysis, and system-level reliability assessment, using polynomial chaos expansion for efficient uncertainty quantification. Furthermore, Chen *et al* [40] introduces a system-level damage-threshold interference model that moves beyond traditional part-to-system analyses by inherently accounting for failure correlations between components within a complex system. To address the high computational cost associated with damage accumulation simulations under uncertainty, surrogate-assisted methods have also been adopted, such as artificial neural networks (ANN), radial basis functions (RBF), and support vector machines (SVM). Qian *et al* [41] carried out fatigue reliability assessment for impellers, using extreme gradient boosting (XGBoost) surrogate to replace computationally expensive finite element simulations, where 400 samples were required for training. Wang *et al* [42] presented a surrogate modeling approach based on the XGBoost surrogate for the creep-fatigue reliability assessment of a low-pressure turbine disk, where the surrogate was trained to establish a high-dimensional mapping between stochastic input parameters and the output creep-fatigue damage, using only 200 high-fidelity finite element samples. In order to enhance the computational efficiency, Gao *et al* [43] proposed an integrated surrogate modeling framework for the creep-fatigue reliability assessment of turbine blades, primarily employing a substructure-based distributed collaborative Kriging model to address multi-source uncertainties and high nonlinearity problems. However, these methods often require a large number of simulations to achieve acceptable accuracy. Recent advances focus on adaptive surrogate modeling (ASM) with active learning strategies to reduce computational burden while maintaining precision. For example, active learning Kriging–Monte Carlo simulation (AK-MCS) method proposed by Echard *et al* [44] and its variants have been successfully applied to structural reliability analysis. In the context of HTRSs, Huang *et al* [45] introduced an active

metamodeling methodology named the multi-layer surrogate control-based synergic enhanced Kriging for efficient and accurate creep-fatigue reliability assessment of turbine disks in aeroengines. To efficiently construct the load cycle–failure probability curve essential for design, Shen *et al* [46] proposed a novel successive AK-MCS method based on an error-based stopping criterion. The training information-sharing strategy reuses samples across different load cycles, dramatically reducing computational cost compared to traditional AK-MCS. Despite these advances, few studies have integrated ASM directly with damage-based time-variant reliability frameworks for HTRSs, especially under multi-source uncertainties spanning both spatial and temporal domains.

To address this, the present work proposes a computational framework for probabilistic damage modeling and reliability assessment of HTRSs. The primary contributions of this work are listed as follows: First, a novel classification is introduced that distinguishing the RVs into random constant amplitude variable (RCAV) and random varied amplitude variable (RVAV) to explore the probabilistic damage accumulations (PDAs) and reliability under different scenarios. Second, a ASM with a new active learning function is developed to enhance computational efficiency and accelerate convergence in PDA analysis. Finally, system-level reliability assessment combining CD-DT criterion with ASM is presented considering multiple weak sites. The remainder of this paper is organized as follows. Section 2 introduces the multi-source uncertainties in HTRSs and categorizes RVs according to their probabilistic properties. Section 3 introduces the proposed reliability assessment by CD-DT criterion incorporating ASM. Numerical simulations and verifications are presented in section 4 to prove its superiority. In section 5, the implementation of the proposed method is demonstrated through its application to a turbine disk, with numerical results verified by MCS. Finally, the main conclusions of this paper are draw in section 6.

2. Multi-sources of uncertainty in HTRS

2.1. Overview

The degradation process of HTRSs is dominated by deterministic physics laws. However, their failure behavior exhibits randomness due to the presence of multi-sources of uncertainty. The physics of failure reveals the damage patterns and provides a foundation for the life design of HTRS, while uncertainty theory focuses on quantifying and analyzing the random responses of HTRS under these uncertain conditions. In engineering practice, safety factors are widely used to receive a conservative design [47, 48]. It is necessary to characterize/quantify the uncertainty by probabilistic model and there are three main sources of uncertainty, including material properties, loading process and structural geometry. Material variability arises from random microstructural differences and microscopic defects. For example, repeated measurements of tensile or yield strength from the same batch of material, even under identical experimental conditions, often yield varying results. Additionally, the startup and shutdown behavior of HTRS, such as rotating speed acceleration rates and dwell times, introduces random variations in loading conditions. Geometric uncertainty, on the other hand, stems from discrepancies between actual dimensions and design specifications due to manufacturing tolerances. In this study, the multi-source uncertainties are treated as aleatory uncertainties, which are inherently random and can be characterized probabilistically through statistical data. While epistemic uncertainties, arising from limited knowledge or modeling approximations, are also relevant in engineering practice, they are not explicitly incorporated in the present framework. The proposed approach, however, is structurally compatible with non-probabilistic uncertainty representations (e.g., evidence theory, fuzzy sets) for future extensions aimed at handling epistemic uncertainty. Given the inevitable introduction of these uncertainties, probabilistic modeling and analysis will be conducted in the following sections.

2.2. Classification of RVs

To model the multi-sources of uncertainty, probabilistic methods are employed to classify the uncertain parameters into RCAVs and RVAVs, based on their probabilistic characteristics over time. The schematic diagram is shown in figure 1. RCAVs are characterized by randomness in their magnitude, but this magnitude remains constant throughout each time (figure 1(a)). Material variability, such as mechanical property parameters, and geometric uncertainties fall into this category. RVAVs, in contrast, not only exhibit random magnitude but also vary in value throughout each cycle (figure 1(b)). Load variations, such as RV loading, are typical examples of RVAVs. By understanding the nature of these uncertainties, we can classify different scenarios of PDA based on three kinds of RV combinations (S1: only RCAVs, S2: only RVAVs and S3: hybrid RVs).

3. Reliability assessment by CD-DT criterion with ASM

This section introduces the proposed time-variant reliability assessment by CD-DT criterion incorporating ASM. Firstly, the damage accumulation process under uncertainties is analyzed considering stochastic loading history. Afterward, the CD-DT criterion is introduced, which serves as the failure criterion for reliability modeling. Then, the ASM is developed to alleviate computational burdens and enhance both efficiency and accuracy. Finally, ASM and CD-DT criterion combined with ASM is applied to compute reliability for a multi-component series system.

3.1. Damage accumulation under uncertainties

Generally, damage can be defined as the degradation of mechanical properties and ultimate failure of materials caused by the formation and propagation of internal micro-defects under

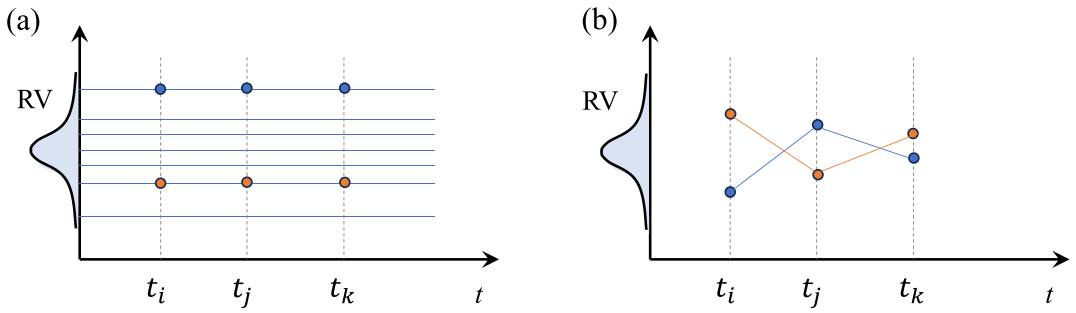

Figure 1. The schematic illustrations for different kinds of RVs: (a) RCAV and (b) RVAV.

external loading. Kachanov [49] proposed the concept of continuum damage mechanics and used to predict the brittle creep fracture time of metallic materials under constant tension. Rabotnov [50] improved Kachanov's theory by introducing a damage variable D, whose physical meaning can be interpreted as the reduction of the effective load-bearing area due to the nucleation and growth of voids. Under the complex loading conditions with varied amplitudes, linear damage summation (LDS) rule can be briefly expressed as:

$$D = \sum_{i=1}^{N} d_i = \sum_{i=1}^{N} \frac{\Delta t_i}{t_{f,i}} t_{f,i} = \alpha^{-1} \cdot s_i^{-n} \tag{1}$$

where $t_{f,i}$, Δt_i, s_i and d_i are the failure lifetime, loading time, stress magnitude and damage at each loading block i under external load F_i, and N is the number of loading blocks. α and n are material constants derived from the stress-life curve. The LDS rule is employed in this work due to its explicit formulation, computational efficiency, and widespread adoption in international design codes [51]. For HTRSs under relatively stable cyclic operation, where load sequence effects are minimal, the LDS rule has been validated as an accurate and practical approach for deterministic life prediction when coupled with energy-based damage models [52]. Its simplicity further facilitates the integration with probabilistic analysis and ASM, allowing efficient uncertainty quantification without sacrificing predictive performance. The damage accumulation becomes a stochastic process due to the randomness of Δt_i and F_i, as illustrated in figure 2. The colored lines represent different possible realizations of the damage path due to randomness in load amplitude and duration (modeled as RVAVs). The pink shaded area illustrates the envelope of these possible trajectories, indicating the dispersion in damage accumulation. The solid line with dots depicts the mean damage path. The consequent distribution in lifetime is indicated by the horizontal spread of points where the individual paths reach the damage threshold D_{th}. Based on the central limit theorem (CLT) [53], the summation of independent and identically distributed RVs will be approximately normally distributed, regardless of the shape of the population distribution, where the expectation and variance of D is formulated as

$$\mu_D = N\mu_d,\ \sigma_D^2 = N\sigma_d^2 \tag{2}$$

where μ_d and σ_d^2 are expectation and variance of d. It is worth noting that accurate calculation of the statistical moments of d is highly difficult, so the first-order Taylor expansion is adopted to obtain an approximate solution. Finally, μ_d and σ_d^2 are expressed as

$$\mu_d \approx \alpha\mu_t(\mu_s)^n \tag{3}$$

$$\sigma_d^2 \approx \alpha^2{\mu_s}^{2n}\left(\sigma_t^2 + \frac{n^2\mu_t^2\sigma_s^2}{{\mu_s}^2}\right) \tag{4}$$

where μ_t, σ_t^2, μ_s, σ_s^2 are expectation and variance of Δt and s, respectively.

3.2. Description of CD-DT criterion

The CD-DT criterion integrates engineering damage mechanics with uncertainty theory to provide failure criteria in the reliability modeling of HTRSs [54, 55]. As seen in figure 3, this criterion is dependent on the understanding to the multi-sources of uncertainty. The cumulative damage, D, which increases over cycles and follows a probability distribution. While the damage threshold, D_{th}, which represents the failure limit, also exhibits randomness due to material variability. Herein, the failure probability is represented by the overlapping area between the PDFs of $D(N)$ and D_{th}. The limit state function (LSF), G, can be constructed by CD-DT criterion, i.e.

$$G = D(N) - D_{\text{th}} \tag{5}$$

where the HTRS is reliable if $G < 0$, and the cumulative damage will not lead to its failure. Thus, the reliability can be evaluated once the probabilistic properties of $D(N)$ and D_{th} are characterized. Considering the situation in figure 2, time-variant reliability $R(N)$ is calculated as

$$R(N) = \Phi(\beta) \tag{6}$$

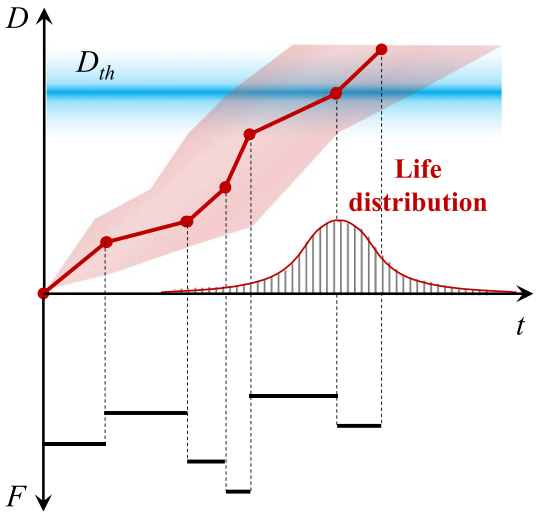

Figure 2. Schematic diagram of damage accumulation under the stochastic loading history.

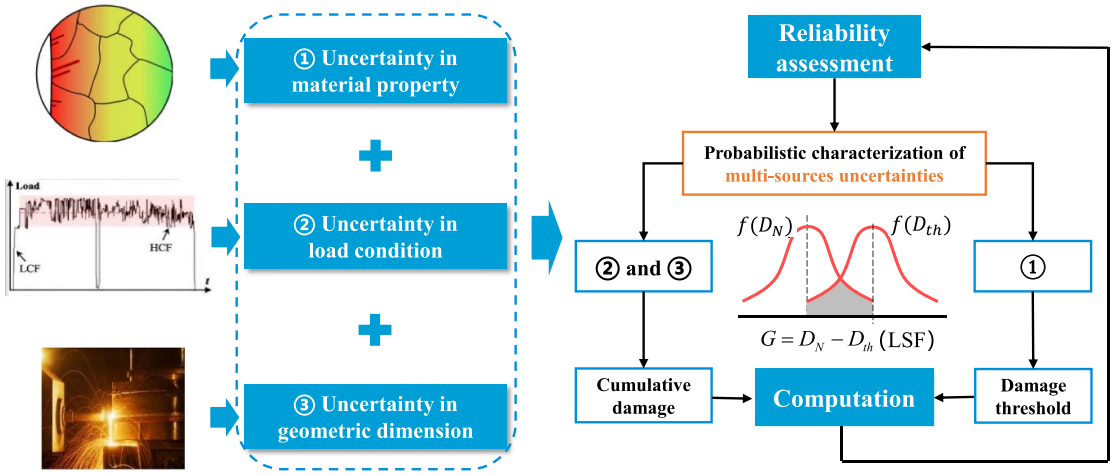

Figure 3. Schematic illustrations of CD-DT interference criterion in reliability assessment of HTRSs considering multi-sources of uncertainty.

$$\beta = \frac{\mu_{D_{\text{th}}} - \mu_D}{\sqrt{\sigma_D^2 + \sigma_{D_{\text{th}}}^2}} \approx \frac{A^{-1}\mu_s{}^{-n}\mu_{D_{\text{th}}} - N\mu_t}{\sqrt{N\left(\sigma_t^2 + n^2\mu_t^2\mu_s{}^{-2}\sigma_s^2\right) + A^{-2}\mu_s{}^{-2n}\sigma_{D_{\text{th}}}^2}} \tag{7}$$

where $D(N)$ and D_{th} are normally distributed RVs, and β denotes reliability index related to N. The reliability index β in equation (6) and its explicit form in equation (7) are derived under the specific condition that both $D(N)$ and D_{th} follow normal distributions. This condition for $D(N)$ arises naturally from the CLT when the damage accumulation is driven by RVAVs over a large number of cycles N. For the damage threshold D_{th}, its normality is supported by empirical evidence from high-temperature fatigue and creep-fatigue tests of GH4169 alloy [34, 56]. It is crucial to note that this analytical form represents a special but practically significant case. The general framework, utilizing Algorithm 1 and MCS, does not rely on this distributional assumption and can handle damage and threshold variables with arbitrary distributions.

3.3. Establishment of ASM

Damage accumulation in actual HTRSs is a very complex and irreversible process that occurs incrementally with time or cycle [52]. LDS rule is employed as

$$D(\mathbf{x}, N) = \sum_{i=1}^{N} d_i(\mathbf{x}) \tag{8}$$

where $D(\mathbf{x}, N)$ represents the accumulated damage at a given cycle, $\mathbf{x}$ is input vector of RVs. In actual damage analysis, $d(\mathbf{x})$ is often highly nonlinear and implicit, requiring time-consuming finite element analysis (FEA). Although MCS is the simplest method to analyze the damage accumulation under uncertainties, its high computational cost, due to the large number of FEA calls, limits its practical use. To mitigate this, Gaussian process regression (GPR) is combined with a novel active learning function, AL($\mathbf{x}$), to construct the ASM. This approach allows for accurate and efficient

Algorithm 1. Procedures to simulate PDA by MCS.

 # Procedure 1 MCS for PDA in S1
Set initial damage accumulation $D = 0$; MCS times K; cycle N;
For $k = 1$: K
  Generate sample (x_1, x_2, x_3) from probabilistic distributions of $\mathbf{x}$;
  Calculate $d(x_1, x_2, x_3)$;
  For $i = 1$: N
    $D = D + d(x_1, x_2, x_3)$; Dam $(i, k) = D$;
  End For
End For
 # Procedure 2 MCS for PDA in S2
For $k = 1$: K
  For $i = 1$: N
    Generate sample (x_1, x_2, x_3) from probabilistic distributions of $\mathbf{x}$;
    Calculate $d(x_1, x_2, x_3)$; $D = D + d(x_1, x_2, x_3)$; Dam $(i, k) = D$;
  End For
End For
 # Procedure 3 MCS for PDA in S3
For $k = 1$: K
  Generate sample x_3 from probabilistic distributions of $\mathbf{x}$;
For $i = 1$: N
    Generate sample (x_1, x_2) from probabilistic distributions of $\mathbf{x}$;
    Calculate $d(x_1, x_2, x_3)$; $D = D + d(x_1, x_2, x_3)$; Dam $(i, k) = D$;
  End For
End For

mapping from RVs to $d(\mathbf{x})$, i.e.

$$\mathrm{AL}(\mathbf{x}) = L(\mathbf{x}) \cdot \sigma(\mathbf{x}) \tag{9}$$

$$L(\mathbf{x}) = \min \left\| \hat{d}(\mathbf{x}), d(\mathbf{x}_m) \right\|_{m \in [1, n_1]} \tag{10}$$

where $\boldsymbol{x}_m$ is the current training input sample, n_1 is the number of training samples, $\hat{d}(\mathbf{x})$ is the predicted damage of one cycle by GPR, $d(\mathbf{x}_m)$ is the actual damage provided by FEA, $\sigma(\mathbf{x})$ represents the standard deviation of predictive result by GPR, and $\|\cdot\|$ denotes the Euclidean distance. In particular, $\sigma(\mathbf{x})$ quantifies the degree of uncertainty in damage prediction, and $L(\mathbf{x})$ quantifies the degree of difference between existing training samples and candidate samples. The candidate sample that maximizes the AL($\mathbf{x}$) is considered as the most valuable sample in this iteration and it should be chosen as the new training sample for updating the surrogate model, known as ASM. The basic principle of GPR is not introduced in this section, interested readers are recommended to [57]. By focusing on only the most informative samples, the ASM significantly reduces the number of FEA calls needed for damage simulation. In addition, the robustness of the proposed ASM framework under different sampling settings is primarily ensured by its active learning mechanism. The learning function AL($\mathbf{x}$) combines prediction uncertainty $\sigma(\mathbf{x})$ with sample novelty $L(\mathbf{x})$ to guide the selection of new training points. This strategy actively explores regions of high uncertainty and fills gaps in the input space, making the model convergence less dependent on the quality of the initial training set. Even if the initial samples are not optimally distributed, the iterative process progressively enriches the training set with the most informative points, driving the predictions of μ_d and σ_d toward stabilization, as demonstrated in following numerical cases. It is important to note that the candidate sample pool S should be sufficiently large and representative of the input variable distributions to enable effective exploration. In practice, monitoring the convergence of the target statistics provides a reliable stopping criterion, ensuring the robustness of the final surrogate model.

The process for constructing the ASM is illustrated in figure 4, with the following steps:

(i) According to the joint probability density function of RVs, generate candidate input sample set S through MCS;
(ii) Select small samples s from S and its output response is evaluated by performance function;
(iii) Construct initial GPR by current training samples, the mean value, μ_d, and standard deviation, σ_d, of $d(\mathbf{x})$ on S are calculated by this model;
(iv) Choose the best next sample from S by AL($\mathbf{x}$) and evaluate its real response;
(v) Add this sample into current training samples;
(vi) Re-train the GPR model based on the updating samples, μ_d, σ_d of $d(\mathbf{x})$ in S are re-calculated;
(vii) Repeat the process until the ASM converges, where the calculations of μ_d, σ_d are stable.

3.4. Computation on time-variant reliability

In engineering applications, HTRSs are typically modeled as multi-component series systems [58]. For instance, the HTRS may have multiple weak sites, such as stress-relief grooves and blade attachments of steam turbine rotors, that are particularly vulnerable to damage. The PDAs of these components are statistically correlated, and the system reliability $R_s(N)$ can be expressed as

$$R_s(N) = P\left(D^1(\mathbf{x}, N) < D_{\mathrm{th}}, D^2(\mathbf{x}, N) < D_{\mathrm{th}}, \ldots, D^M(\mathbf{x}, N) < D_{\mathrm{th}}\right) \tag{11}$$

where $D^M(\mathbf{x}, N)$ denotes the PDA of Mth component in system after N cycle. In this analysis, the LSF for this series systems can be expressed as

$$G(\mathbf{x}, N) = \begin{cases} \geqslant 0, & \forall (D^m(\mathbf{x}, N) \leqslant D_{\mathrm{th}}) \\ < 0, & \exists (D^m(\mathbf{x}, N) > D_{\mathrm{th}}) \end{cases}, m = 1, 2, \ldots, M. \tag{12}$$

As it indicates that the LSF constructed for reliability assessment of HTRS is time varied, and the HTRS is safety when $G(\mathbf{x}, N) \geqslant 0$. Afterward, the reliability is calculated by using ASM-based MCS, expressed as

$$R_s(N) = \frac{\sum_{k=1}^{K} I_k}{K} \tag{13}$$

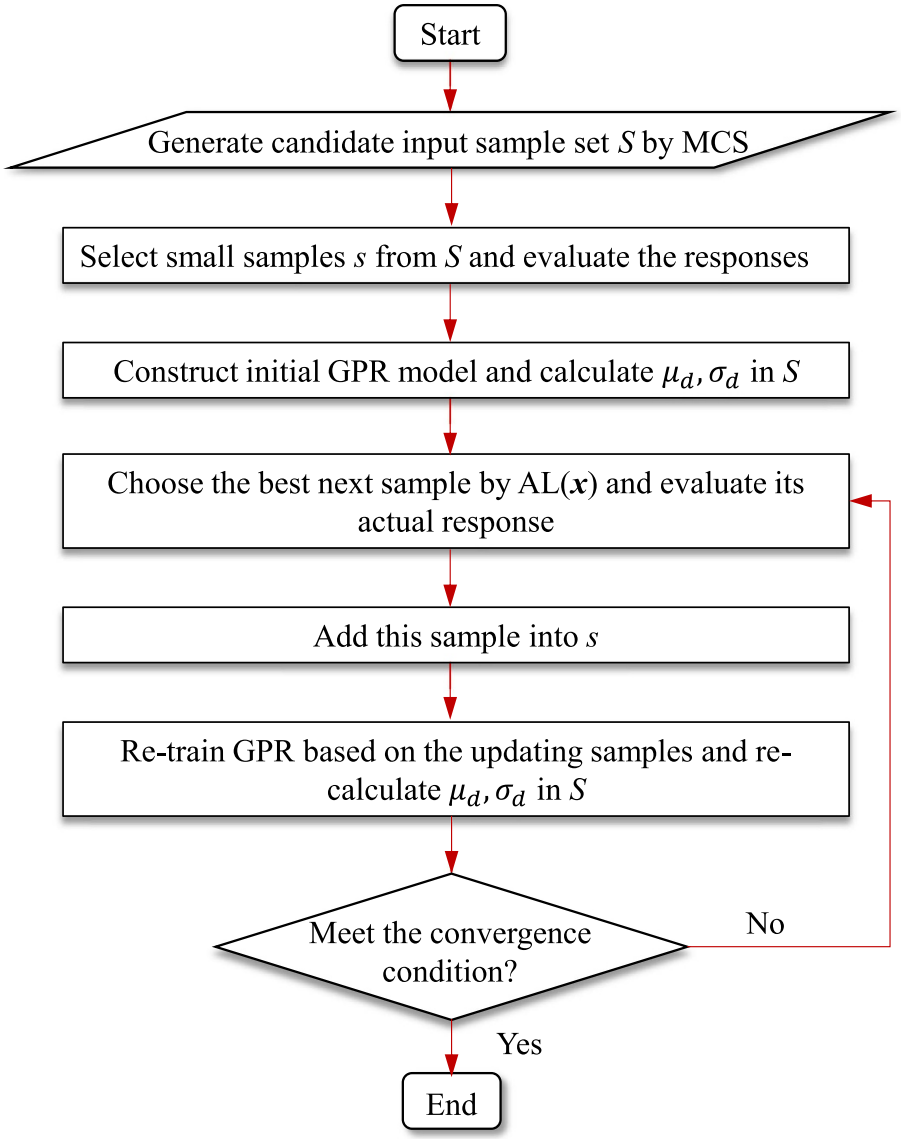

Figure 4. Flow chart of constructing the ASM, reducing the number of FEA calls needed for accurate simulation.

$$I_k = \begin{cases} 1, & G(\mathbf{x}_k, N) \geqslant 0 \\ 0, & G(\mathbf{x}_k, N) < 0 \end{cases} \tag{14}$$

where $\mathbf{x}_k$ is the kth sample of input variables, K is the MCS times, I denotes the safety indicator function. It should be noted that $D^m(\mathbf{x}_k, N)$ can be simulated by the ASM, and thus the reliability assessment is convenient.

4. Numerical simulations and verifications

4.1. Simulation and verification of PDA

According to section 2.2, the external load and the duration time are treated as RVAVs (Scenario S2). Alternatively, they can be modeled as RCAVs (Scenario S1), or as hybrid RVs (Scenario S3). Each Scenario leads to distinct damage-accumulation trajectories and probabilistic characteristics. The numerical case is presented to explore the PDA for the scenarios S1–S3. For illustrative purposes, the damage function $d(\mathbf{x})$ is given by following mathematical expression

$$d(\mathbf{x}) = \frac{x_1^2 + x_1 x_3 + x_2^2}{1000} \tag{15}$$

where x_1, x_2, x_3 are normal RVs. Their mean values are $\mu_{x1} = 1$, $\mu_{x2} = 2$, and $\mu_{x3} = 0$, their standard deviations are $\sigma_{x1} = 0.5$, and $\sigma_{x3} = 1$. $d_i(\mathbf{x})$ denotes the damage in ith cycle under the uncertainty inputs. For clarity, procedures to simulate PDA from S1 to S3 are given as follows.

The MCS results of PDA to $N = 100$ cycles ($K = 10$) under different scenarios are shown in figures 5(a)–(c). The results demonstrate variations in damage accumulations, represented by colored lines that show different trajectories. The results demonstrate that the dispersion of PDA varies significantly across different scenarios. Specifically, the PDA in S1 displays

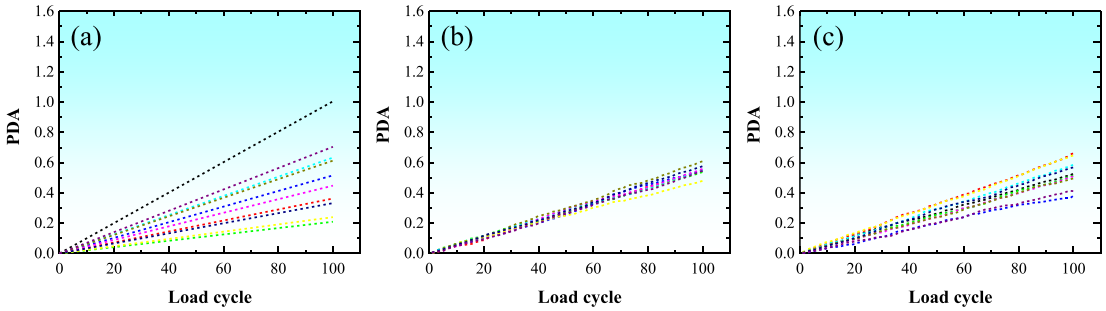

Figure 5. MCS results of PDA to $N = 100$ cycles ($K = 10$) for the scenarios of (a) S1, (b) S2, and (c) S3.

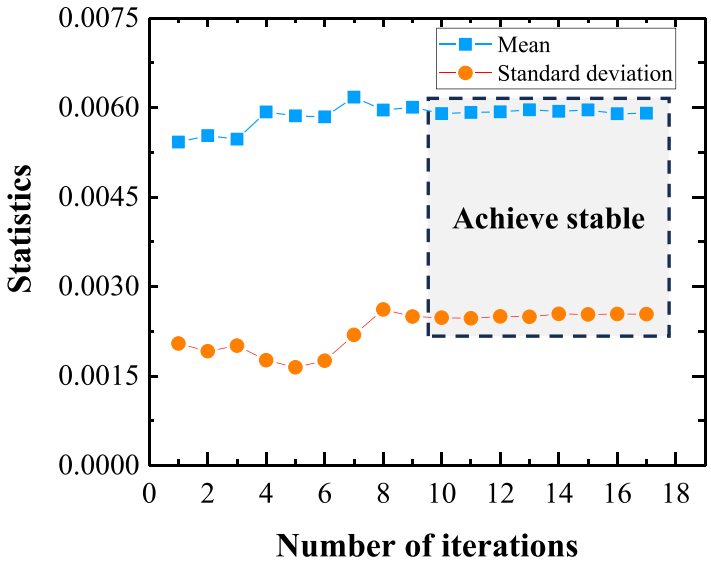

Figure 6. Iterative convergence process of the ASM for the benchmark case ($d(\mathbf{x})$ from equation (15)). The predicted mean (μ_d) and standard deviation (σ_d) of the damage per cycle stabilize as samples are added via the active learning function.

the greatest level of scattering, indicating that the probability of failure is highest in this scenario. Based on the CLT, the PDAs in S2 and S3 are normally distributed, while the distribution of PDA in S1 cannot be determined in advance until the MCS results are available. This will be confirmed by the following large-scale MCS results.

Afterward, the above numerical case given by equation (15) is conducted to verify the accuracy and efficiency of the ASM in comparison to MCS. 7 training samples are generated firstly to train the initial GPR model. Then, GPR is re-trained by the updated training samples by active learning function, μ_d, σ_d are re-calculated at each iteration until the values are stable, as seen in figure 6. Finally, ASM is established with a total of 23 samples (7 initial samples + 16 new samples) that they need to call equation (15).

In order to further verify the constructed ASM in approximating $d(\mathbf{x})$, five commonly used models i.e. ANN, RBF, extreme learning machine (ELM), SVM and GPR (without adaptive learning process) are also presented for comparison. It should be noted that the five models are trained using the same number of samples, and the simulated results are listed in table 1, where the statistics of $d(\mathbf{x})$ such as mean value, standard deviation, kurtosis and skewness are included. As it shows that the ASM has the smallest average relative error (RE) among the four statistical measures, with the 10^5 MCS considered as 'exact' solutions. According to the procedures for simulating PDA in S1–S3, the MCS results of PDA at $N = 100$ cycles ($K = 10^5$) are presented in figures 7(a)–(c), the simulated results by ASM are provided in figures 7(d)–(f).

The results confirm that PDA in scenarios S2 and S3 follows a normal distribution, while the PDA in S1 does not necessarily exhibit normality. The mean value and standard deviation of PDA in all scenarios (S1–S3) are listed in table 2, where the RE of the statistics calculated using ASM are below 7%. In addition, it can be understood that the reliability assessment in different scenarios may vary due to the different distributions of PDA, which will be explored in section 4.2.

4.2. Simulation and verification of reliability

To verify the accuracy and efficiency of ASM-based MCS for time-variant reliability assessment, a numerical case study is performed. A series system with two components is simulated,

Table 1. Comparisons of different models to approximate the distribution of $d(\mathbf{x})$.

Model	Mean	Standard deviation	Kurtosis	Skewness	Average RE (%)
MCS	**0.0055**	**0.0026**	**3.6704**	**0.6556**	—
ANN	0.0057	0.0021	2.7170	−0.3514	50.61
RBF	0.0062	0.0022	2.1605	−0.1056	46.34
ELM	0.0054	0.0027	3.1587	0.0406	28.35
SVR	0.0052	0.0019	2.9296	0.2321	29.29
GPR	0.0053	0.0023	2.9536	0.0172	33.02
ASM	0.0058	0.0026	3.3838	0.5649	6.77

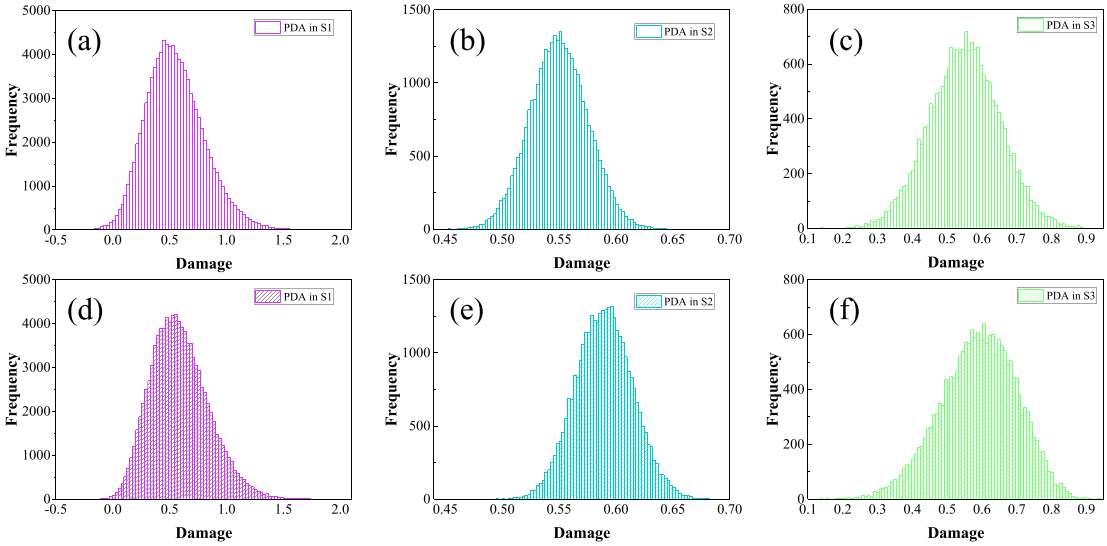

Figure 7. Result comparisons between MCS and ASM in different scenarios (a)–(c) MCS in S1–S3, and (d)–(f) ASM in S1–S3.

Table 2. Summary of the statistics of PDA at $N = 100$ cycles.

Scenario	Mean (MCS)	Mean (ASM)	Standard deviation (MCS)	Standard deviation (ASM)	Average RE (%)
S1	0.5509	0.5896	0.2552	0.2525	4.04
S2	0.5499	0.5896	0.0255	0.0252	4.20
S3	0.5504	0.5899	0.1030	0.1097	6.84

where $d_1(\mathbf{x})$, $d_2(\mathbf{x})$, are given by

$$d_1(\mathbf{x}) = \frac{x_1^2 + x_1 x_3 + x_2^2}{1000},\ d_2(\mathbf{x}) = \frac{x_1^2 + x_2^2 + x_3^2}{1000} \tag{16}$$

where x_1, x_2, x_3 are normally distributed RVs with means $\mu_{x1} = 1$, $\mu_{x2} = 2$, and $\mu_{x3} = 0$, and standard deviations $\sigma_{x1} = 0.5$, $\sigma_{x2} = 0.5$, $\sigma_{x3} = 1$, and D_{th} is normally distributed with $\mu_{D_{\text{th}}} = 1$ and $\sigma_{D_{\text{th}}} = 0.15$. Similarly, the ASM is trained using 21 samples (7 initial samples + 14 added samples) for the two-component system defined by equation (16), and the convergence process of the ASM during this training is shown in figure 8.

The calculation results of reliability at $N = 100$ cycles are listed in table 3 and they are compared with the MCS results ($K = 10^5$). In the proposed reliability assessment, only 21 calls are required, compared with 10^5 calls in MCS. In addition, five commonly used models such as ANN, RBF, ELM, SVM and GPR are included for comparison, from which the five models are trained using the same number of samples. Considering MCS results as 'exact' solutions, the ASM-based method shows the best prediction performance among these models, where the average RE of the reliability calculations by ASM in all scenarios (S1–S3) are lower than 2%. The proposed reliability assessment greatly improves efficiency while presenting satisfactory accuracy. In addition, the reliability values in table 3 exhibit clear differences across scenarios S1–S3. This is a direct consequence of the distinct PDA behaviors induced by different RV combinations. In S1 (only RCAVs), the damage accumulation shows the highest dispersion (figure 5(a)), leading to the highest probability of exceeding the damage threshold and thus the lowest reliability. In S2 (only RVAVs), the damage accumulation, guided by the CLT, converges toward a normal distribution with much smaller variance (figure 5(b)), resulting in higher reliability. Scenario S3, with hybrid RVs, presents an intermediate case both in

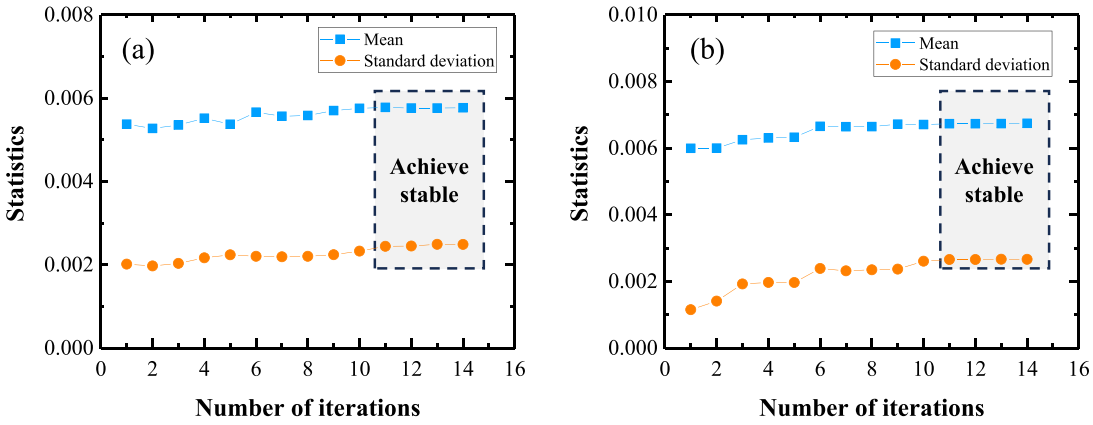

Figure 8. Iterative and convergence processes of the ASM during its training for the two-component series system case (damage functions from equation (16)).

Table 3. Summary of reliability assessment at $N = 100$ cycle for S1, S2 and S3 by different models.

Model	S1	S2	S3	Average RE (%)
MCS	**0.8670**	**0.9897**	**0.9460**	—
ANN	0.9022	0.9953	0.9813	2.79
RBF	0.9502	0.9946	0.9898	4.91
ELM	0.8456	0.9804	0.9169	2.16
SVR	0.8986	0.9813	0.9708	2.37
GPR	0.8981	0.9914	0.9688	2.06
ASM	0.8462	0.9843	0.9292	1.57

terms of PDA dispersion and the resulting reliability. These comparisons validate the necessity of classifying RVs based on their temporal probabilistic characteristics for accurate reliability assessment.

5. Application in a turbine disk

5.1. Implementation procedures

In this section, probabilistic damage modeling and reliability assessment of a low-pressure turbine disk subjected to creep-fatigue damage are presented as an engineering case study to illustrate the implementation of the proposed method. Figure 9 outlines the implementation steps. This flowchart enables accurate and efficient assessment of reliability of the turbine disk throughout its operational life.

The first step in the process is to identify the weakest regions in the turbine disk, which are most susceptible to failure due to high levels of creep-fatigue damage. FEA simulates the turbine disk's mechanical and thermal behaviors under the operational conditions it encounters during flight tasks. The turbine disk is subjected to centrifugal forces generated by rotational speed and temperature gradients during its operation. Creep and fatigue damage models are implemented using user subroutines to capture the combined damage accumulation over repeated cycles of takeoff, cruising, and landing. The second step involves quantifying the uncertainties inherent in the turbine disk's material properties, geometric dimensions, and operational loading conditions. These uncertainties arise from variations in microstructure, manufacturing processes, and the stochastic nature of operating conditions such as rotating speed and dwell time.

The probability distributions of these RVs are established through statistical analysis of experimental data and expert knowledge. In the third step, ASM is established to reduce the computational complexity of the probabilistic damage analysis, and to approximate the relationship between the random inputs and the damage output at each weak site. A small set of training samples is generated initially using Latin hypercube sampling, ensuring a broad coverage of the input space. The active learning function then selects the most informative new samples to iteratively call the FEA, focusing computational resources on the most critical areas of the input space. This iterative process continues until the ASM converges. Finally, it involves using the established ASM to quantify the PDA at the identified weak sites and assess the reliability. The CD-DT interference criterion is applied to evaluate the likelihood that the accumulated damage at any weak site exceeds a critical threshold.

5.2. Weakness identification of turbine disk

The 3D model of turbine disk in aeroengine is presented in figure 10(a), with a total of 72 blades assembled at disk rim by fir-tree groove structures. Considering the symmetrical characteristic and huge computational burden in the following FEAs, 1/72 sector of a 2D FE model of disk is constructed in ABAQUS, where the mesh generation is shown in figure 10(b). The mesh independent tests and convergency analysis are carried out to ensure the accuracy of FE model, and CAX4R element type is adopted for a total of 7413 elements. Boundary conditions are applied to the 2D FE model of turbine disk, as shown in figure 10(b). The mechanical boundary condition is imposed through the centrifugal force from blades and disk

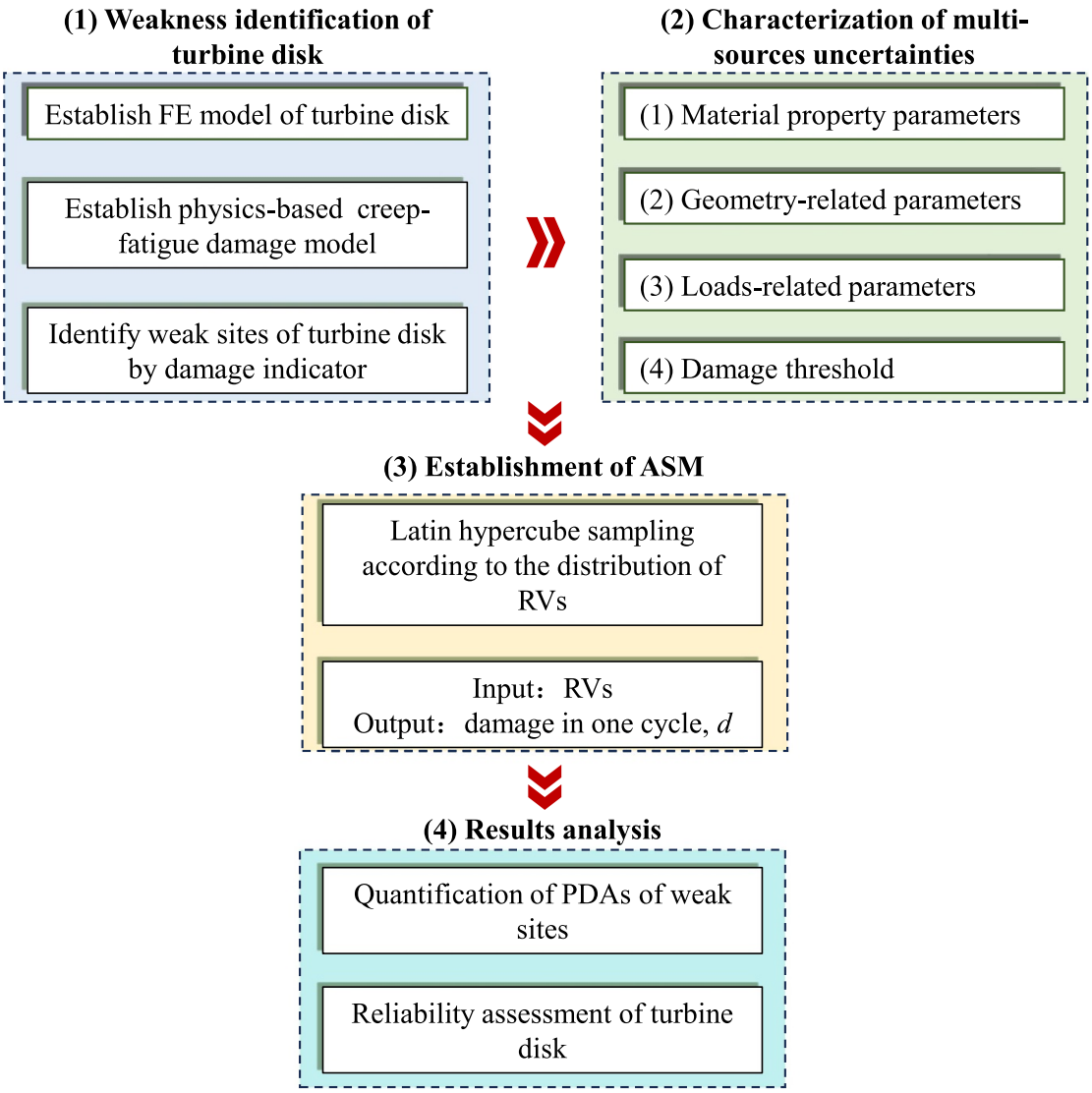

Figure 9. Implementation procedures for the engineering case study based on the proposed method incorporating ASM and CD-DT criterion.

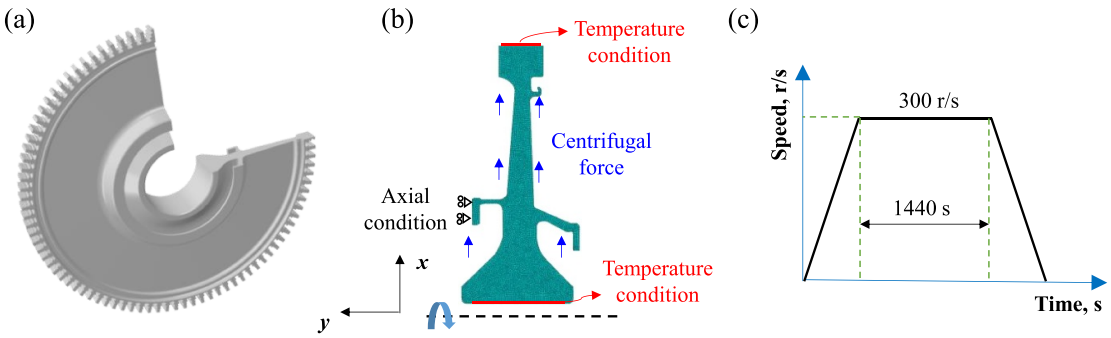

Figure 10. Finite element modeling of turbine disk using ABAQUS (a) 3D model, (b) mesh generation of FE model, and (c) simplified load history curve of turbine disk in one flight task.

itself, where the centrifugal force is set with the Y-axis as the rotating axis. The minimum temperature is set as 450 °C at the shaft end, the maximum temperature is set as 580 °C at the disk rim. In addition, the load history curve of turbine disk in one flight task is given in figure 10(c), where the mean values of rotating speed and dwell time are 300 r s^{-1} and 1440 s, respectively. Subsequently, the non-unified constitutive models involving strain hardening creep model and elastoplastic

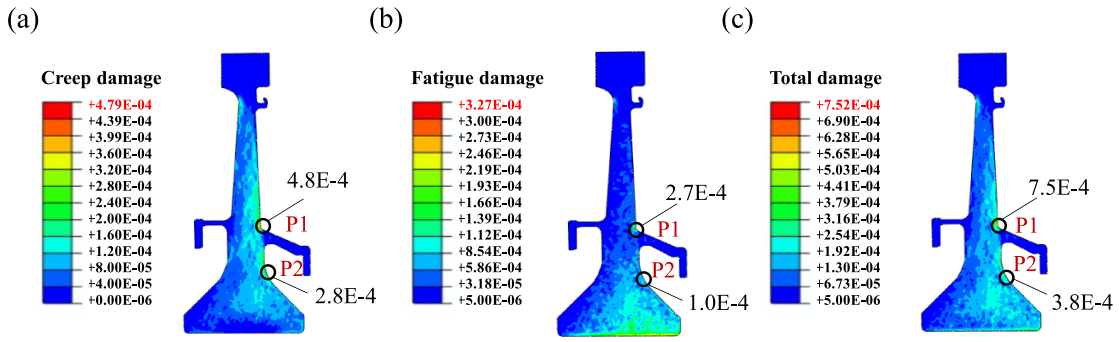

Figure 11. FEA results presented by cloud plot of (a) creep damage in one cycle, (b) fatigue damage in one cycle, and (c) total damage in one cycle.

fatigue model are adopted for stress-strain analysis [59], the damage in one cycle is quantified by strain energy density exhaustion model with the input of stress-strain response [60]. The model parameters of disk material at different temperatures, which are used for FEA, had been listed in [42].

FEA results for creep, fatigue, and total damage after one cycle are shown in figures 11(a)–(c). The weaknesses are identified as some sites of turbine disk with a larger magnitude of damage, wherein the results show that P1and P2 should be regarded as the weakest sites that have the risks to failure after a certain number of cycles. The time-variant reliability assessments are detailed in section 5.5.

5.3. Characterization of multi-sources uncertainties

The material variability led to the scattered experimental lifetimes under the same load conditions, according to the statistical analysis of creep-fatigue data of IN718 superalloy, D_{th} is determined as a normally distributed variable with mean value of 1 and standard deviation of 0.15 [34]. The mechanical property parameters involving material density ρ, Yong's module E, thermal conductivity λ and expansion coefficient α have randomness, they are RCAVs. The load-related parameters, such as the rotational speed ω and cruising time t_d, are modeled as RCAVs in this case study. This treatment is based on the operational context of a commercial aircraft engine, which typically executes standardized, repeated flight missions (takeoff-cruise-landing). Under such a regime, the load history exhibits minor random variations from one mission to another but remains relatively constant within a given mission simulation. It is crucial to note that this 'RCAV-for-loads' assumption is specific to stable, repetitive operational profiles and should not be generalized to components under strongly non-stationary conditions, where load parameters would more appropriately be modeled as RVAVs. Two typical dimensions of the turbine disk c_1 and c_2 are selected to account for the geometric uncertainty, where they are RCAVs. Therefore, only RCAVs (S1) are involved in the application to turbine disk. Afterwards, a normal distribution is adopted to represent the probabilistic distribution to quantify the uncertainty of these parameters, where they are modeled by the coefficient of variation (CV), as summarized in table 4.

Table 4. Uncertainty inputs of material parameters, geometric dimension parameters and loading condition parameters for the turbine disk.

Category	Parameter	Mean value	Unit	CV
Material property	ρ	8240	Kg m^{-3}	0.01
	E	182	GPa	0.05
	λ	30.4	W (m· °C)$^{-1}$	0.01
	α	1.87×10^{-5}	K^{-1}	0.01
Geometry	c_1	9.2	mm	0.000 33
	c_2	76.7	mm	0.000 33
Loads	ω	300	r s^{-1}	0.01
	t_d	1440	s	0.01

5.4. Establishment of ASM

In order to construct the ASM, 20 initial samples are generated from the RVs listed in table 4, and FEAs are performed to create the input–output dataset. The input variables represent the uncertainty sources, while the output is the damage per cycle at the identified weak sites. The inputs are normalized using dimensionless methods to accelerate convergence. The iterative process of the ASM construction is shown in figure 12, where additional samples are selected using the active learning function. The process converged after 30 iterations, and the mean and standard deviation of the damage at the weak sites are calculated using the ASM. To verify the accuracy of the ASM, MCS was also performed. Figure 13 compares the damage assessment results between MCS and ASM, with REs below 20%, confirming the accuracy and efficiency of the ASM. Notably, the ASM requires only 50 times of FEA, compared to 10 000 in MCS, significantly enhancing computational efficiency.

5.5. Reliability assessment

The ASM is used to quantify the PDA of the identified weak sites, corresponding to the case in scenario S1 (see section 3.1). To examine the evolutions of PDAs with cycle, the PDF curves of PDAs for P1-P3 are plotted in figure 14. These curves show the evolutions of damage over 100, 300, and

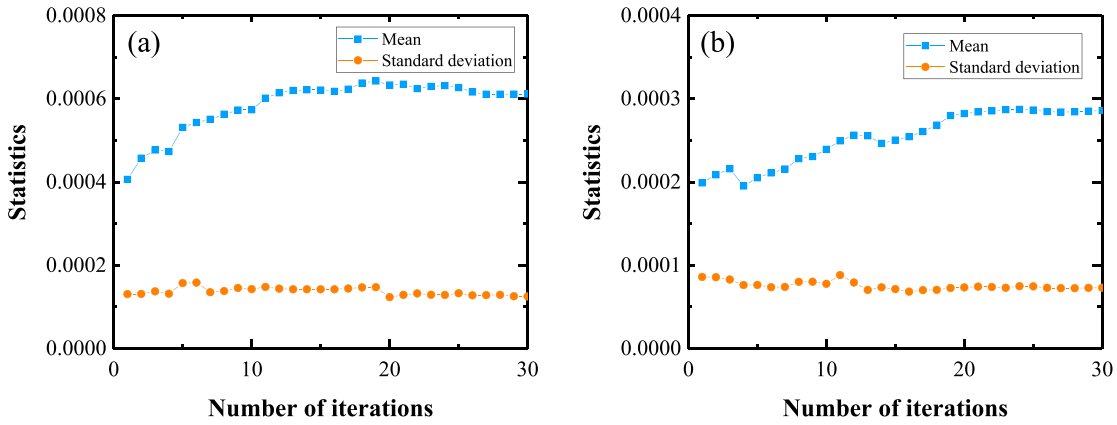

Figure 12. Iterative processes of ASM to approximate the mean and standard deviation of damage of two weak sites (a): P1 and (b): P2.

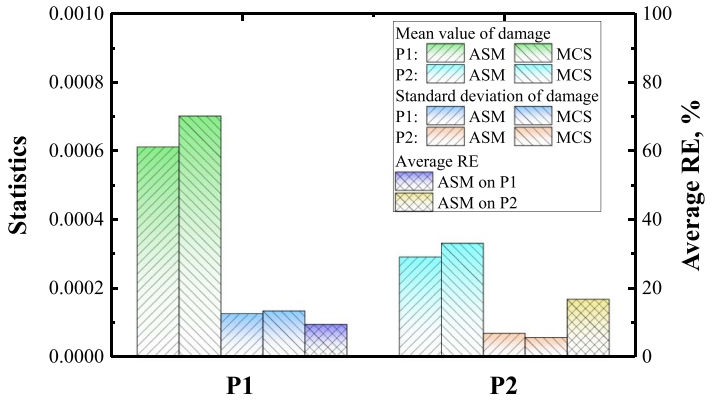

Figure 13. Full comparisons of MCS and ASM for the damage magnitudes based on two weakness sites in turbine disk.

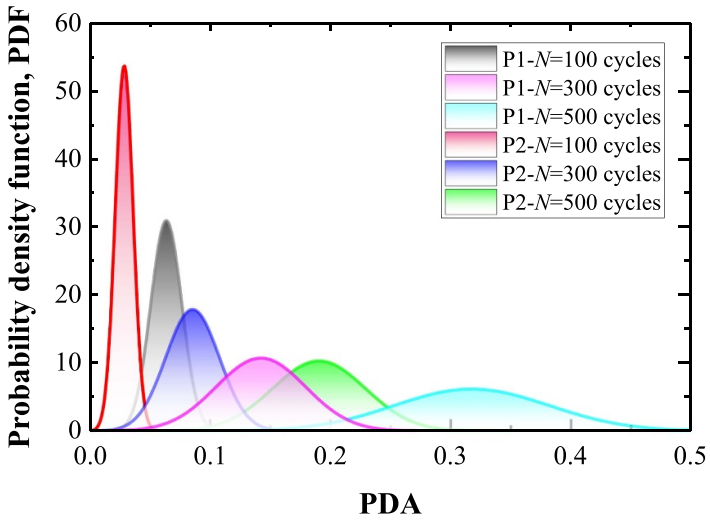

Figure 14. Evolutions of PDAs for two weakness sites P1 and P2 at different cycles.

500 cycles, each represented by a colored line. As it indicates that both the expectation and variance of PDA are increased with cycle. Site P1 exhibited the greatest scatter in damage accumulation, indicating that it poses the highest risk of failure.

The system reliability of turbine disk at different design cycles are calculated by ASM and other popular used surrogates, as listed in table 5. Result shows that the reliability degree decrease with the rise of design cycles, and the reliabilities of turbine disk are 98.41%, 97.30% and 95.85%,

Table 5. Reliability prediction precision of turbine disk with different models.

Cycle	MCS	ANN	RBF	ELM	SVR	GPR	ASM	Average RE (%)
850	0.9841	0.9923	0.9901	0.9929	0.9926	0.9795	0.9872	2.98 (ANN)
900	0.973	0.9854	0.9822	0.9869	0.9873	0.9685	0.9784	1.04 (RBF)
950	0.9585	0.9788	0.9694	0.977	0.978	0.9533	0.9593	2.88 (ELM)
1000	0.9308	0.9601	0.943	0.9621	0.9611	0.9304	0.9348	2.96 (SVR)
1050	0.9008	0.9405	0.911	0.9387	0.9412	0.9065	0.8994	0.81 (GPR)
1100	0.8586	0.9112	0.8682	0.9053	0.9069	0.8816	0.8538	0.35 (ASM)

respectively at the designed cycles of $N = 850$, 900 and 950 considering the multi-sources of uncertainty. The last column of table 5 provides the predictive precisions of five surrogates and ASM, where the crude MCS ($K = 10^4$) is regarded as the benchmark. In particular, the average RE of ASM is less than 0.5% compared to MCS, which is superiors to other surrogates. More importantly, this study offers valuable insights into damage-driven reliability assessment of HTRSs and has significant potential for the applications in more complex structural systems.

6. Conclusions

In this work, a computational framework for time-variant reliability assessment of HTRSs has been developed, addressing the challenges posed by multi-source uncertainties. The proposed framework integrates the principles of engineering damage mechanics with uncertainty quantification and ASM. Several numerical case studies and a practical application to a turbine disk have verified the effectiveness of this developed method. The main findings are summarized as follows:

(1) The uncertain parameters in HTRSs are classified into RCAV and RVAV, enabling the distinction between damage accumulation. The PDAs under three scenarios (S1, S2, and S3) exhibit significant differences, emphasizing the importance of correctly identifying the nature of uncertainties.
(2) To alleviate the high computational cost of traditional MCS, an ASM is constructed. The ASM effectively approximates the relationship between RVs and damage accumulation, significantly reducing the number of finite element analysis calls required. This approach demonstrates high efficiency while maintaining accuracy, with REs below 2% compared to MCS results.
(3) The proposed method is applied to a low-pressure turbine disk subjected to creep-fatigue damage. Material variability, load variations, and geometric uncertainties are quantified and incorporated into the analysis. The reliability assessment shows that the turbine disk has a reliability degree of 98.41% at a design life of 850 cycles, with REs less than 0.5% when compared to MCS results, confirming the accuracy and applicability of the method in particular engineering applications.

Despite its demonstrated effectiveness, the proposed framework has certain limitations that suggest directions for future research. Firstly, the computational efficiency of the ASM may decrease for problems with very high-dimensional uncertainty inputs. Exploring more scalable surrogate models or ensemble methods is a promising avenue for improvement. Secondly, the current methodology is built upon a probabilistic framework for aleatory uncertainties. Its extension to incorporate epistemic uncertainties using non-probabilistic methods would enhance its applicability. Finally, while the LDS rule is suitable for the studied cases, integrating more advanced nonlinear damage accumulation models could broaden the validity of this framework for components under complex load sequences. Addressing these aspects will be the focus of subsequent studies.

Acknowledgments

This work was supported by MEXT Strategic Professional Development Program for Young Researchers of Japan (TIFRIS Fellow, No. J250000163), and NEXUS Program of Japan's First University for International Research Excellence.

ORCID iD

Run-Zi Wang 0000-0002-9483-8407

References

[1] Unnikrishnan U and Yang V 2022 A review of cooling technologies for high temperature rotating components in gas turbine *Propuls. Power Res.* **11** 293–310
[2] Moroz L, Doerksen G, Romero F, Kochurov R and Frolov B 2017 Integrated approach for steam turbine thermo-structural analysis and lifetime prediction at transient operations *Turbo Expo: Power for Land, Sea, and Air* (American Society of Mechanical Engineers) pp V008T29A12
[3] Moroz L, Frolov B and Kochurov R 2016 Steam turbine rotor transient thermo-structural analysis and lifetime prediction *Turbo Expo Power for Land, Sea, and Air* (American Society of Mechanical Engineers) p V008T26A38
[4] Adamson K M, Walmsley T G, Carson J K, Chen Q, Schlosser F, Kong L and Cleland D J 2022 High-temperature and transcritical heat pump cycles and advancements: a review *Renew. Sustain. Energy Rev.* **167** 112798
[5] Wechsung M, Feldmüller A and Lemmen H 2012 Steam turbines for flexible load operation in the future market of power generation *Turbo Expo: Power for Land, Sea and Air* American Society of Mechanical Engineers) pp 579–88

[6] Lefton S, Edmonds J, Foulds J and Montrose J Effects of flexible operation on turbines and generators *Technical Report* (Electric Power Research Institute) p 1008351
[7] Su L, Wen F, Wang S and Wang Z 2022 Analysis of energy saving and thrust characteristics of rotating detonation turbine engine *Aerosp. Sci. Technol.* **124** 107555
[8] Grell W A and Laz P J 2010 Probabilistic fatigue life prediction using AFGROW and accounting for material variability *Int. J. Fatigue* **32** 1042–9
[9] Sankararaman S, Ling Y, Shantz C and Mahadevan S 2011 Inference of equivalent initial flaw size under multiple sources of uncertainty *Int. J. Fatigue* **33** 75–89
[10] Wang X, Mignolet M P and Soize C 2020 Structural uncertainty modeling for nonlinear geometric response using nonintrusive reduced order models *Probab. Eng. Mech.* **60** 103033
[11] Zhu S P, Liu Q, Zhou J and Yu Z Y 2018 Fatigue reliability assessment of turbine discs under multi-source uncertainties *Fatigue & Fracture of Engineering Materials & Structures* p 41
[12] An Z W, Huang H Z and Liu Y 2008 A discrete stress–strength interference model based on universal generating function *Reliab. Eng. Syst. Saf.* **93** 1485–90
[13] Gao J, An Z and Liu B 2016 A dependent stress–strength interference model based on mixed copula function *J. Mech. Sci. Technol.* **30** 4443–6
[14] Li Y, Chen J, Liu J, Zhang L, Wang W and Zhang S 2013 Estimation of the reliability of all-ceramic crowns using finite element models and the stress–strength interference theory *Comput. Biol. Med.* **43** 1214–20
[15] Frangopol D M, Strauss A and Kim S 2008 Bridge reliability assessment based on monitoring *J. Bridge Eng.* **13** 258–70
[16] Strutt J, Allsopp K and Ouchet L 1995 Reliability prediction of pipes and valves *Qual. Reliab. Eng. Int.* **11** 91–100
[17] Fang Y, Tao W and Tee K F 2019 A new computational method for structural reliability with big data *Eksploatacja I Niezawodnosc.* **21** 159–63
[18] Nadarajah S 2005 Reliability for some bivariate gamma distributions *Math. Probl. Eng.* **2005** 151–63
[19] Longbiao L 2017 Modeling strength degradation of fiber-reinforced ceramic-matrix composites under cyclic loading at room and elevated temperatures *Mater. Sci. Eng.* **695** 221–9
[20] Liu X, Zhang W, Gu X and Zeng Y 2017 Degradation of mechanical behavior of corroded prestressing wires subjected to high-cycle fatigue loading *J. Bridge Eng.* **22** 04017004
[21] Van Paepegem W and Degrieck J 2002 A new coupled approach of residual stiffness and strength for fatigue of fibre-reinforced composites *Int. J. Fatigue* **24** 747–62
[22] D'Amore A, Giorgio M and Grassia L 2015 Modeling the residual strength of carbon fiber reinforced composites subjected to cyclic loading *Int. J. Fatigue* **78** 31–37
[23] Wang J and Qiu Z P 2012 Fatigue reliability based on residual strength model with hybrid uncertain parameters *Acta Mech. Sin.* **28** 112–7
[24] Philippidis T and Passipoularidis V 2007 Residual strength after fatigue in composites: theory vs. experiment *Int. J. Fatigue* **29** 2104–16
[25] Post N, Cain J, McDonald K, Case S W and Lesko J 2008 Residual strength prediction of composite materials: random spectrum loading *Eng. Fract. Mech.* **75** 2707–24
[26] Son Y K 2011 Reliability prediction of engineering systems with competing failure modes due to component degradation *J. Mech. Sci. Technol.* **25** 1717–25
[27] Zhang X, Gao H, Huang H Z, Li Y F and Mi J 2018 Dynamic reliability modeling for system analysis under complex load *Reliab. Eng. Syst. Saf.* **180** 345–51
[28] Xin T, Zhao J, Cui C and Duan Y 2020 A non-probabilistic time-variant method for structural reliability analysis *Proc. Inst. Mech. Eng. O* **234** 664–75
[29] Yuan R, Li H, Huang H Z, Zhu S P and Gao H 2015 A nonlinear fatigue damage accumulation model considering strength degradation and its applications to fatigue reliability analysis *Int. J. Damage Mech.* **24** 646–62
[30] Huang H Z and An Z W 2008 A discrete stress-strength interference model with stress dependent strength *IEEE Trans. Reliab.* **58** 118–22
[31] Schaff J R and Davidson B D 1997 Life prediction methodology for composite structures. Part I—constant amplitude and two-stress level fatigue *J. Compos. Mater.* **31** 128–57
[32] Yao W and Himmel N 2000 A new cumulative fatigue damage model for fibre-reinforced plastics *Compos. Sci. Technol.* **60** 59–64
[33] Gao J and An Z 2019 A new probability model of residual strength of material based on interference theory *Int. J. Fatigue* **118** 202–8
[34] Wang R Z, Gu H H, Zhu S P, Li K S, Wang J, Wang X W, Hideo M, Zhang X-C and Tu S-T 2022 A data-driven roadmap for creep-fatigue reliability assessment and its implementation in low-pressure turbine disk at elevated temperatures *Reliab. Eng. Syst. Saf.* **225** 108523
[35] Gu H H, Wang R Z, Tang M J, Zhang X C and Tu S T 2023 Creep-fatigue reliability assessment for high-temperature components fusing on-line monitoring data and physics-of-failure by engineering damage mechanics approach *Int. J. Fatigue* **169** 107481
[36] Gu H H, Wang R Z, Tang M J, Zhang X C and Tu S T 2023 Data-physics-model based fatigue reliability assessment methodology for high-temperature components and its application in steam turbine rotor *Reliab. Eng. Syst. Saf.* **241** 109633
[37] Kong C, Jin J S, Lin K B, Jiang Y W and Chen S T 2025 Fatigue damage accumulation model of a high-pressure oil pipe based on fatigue probability under Multi-Level cyclic loading *Eng. Fract. Mech.* **316** 110899
[38] Peng Z C, Shi L M, Hu J, Jiang Q Q and Wu J 2024 Probabilistic modeling of double linear damage accumulation and its application in fatigue reliability analysis *Qual. Reliab. Eng. Int.* **40** 2196–215
[39] Gu H H, Wang R Z, Zhang K, Li K S, Sun L and Zhang X C 2025 Damage-driven framework for reliability assessment of steam turbine rotors operating under flexible conditions *Reliab. Eng. Syst. Saf.* **254** 110578
[40] Chen J P, Zhao B F, Zhang K, Xie L Y, Zhang X C, Wang R Z and Sun W-Q 2025 System-level damage-threshold interference model for system reliability evaluation *Reliab. Eng. Syst. Saf.* **262** 111184
[41] Qian C, Li W J, Wei S X, Sun B and Ren Y 2024 Fatigue reliability evaluation for impellers with consideration of multi-source uncertainties using a WOA-XGBoost surrogate model *Qual. Reliab. Eng. Int.* **40** 3193–211
[42] Wang R Z, Gu H H, Liu Y, Miura H, Zhang X C and Tu S T 2023 Surrogate-modeling-assisted creep-fatigue reliability assessment in a low-pressure turbine disc considering multi-source uncertainty *Reliab. Eng. Syst. Saf.* **240** 109550
[43] Gao H F, Wang Y H, Li Y and Zio E 2024 Distributed-collaborative surrogate modeling approach for creep-fatigue reliability assessment of turbine blades considering multi-source uncertainty *Reliab. Eng. Syst. Saf.* **250** 110316
[44] Echard B, Gayton N and Lemaire M 2011 AK-MCS: an active learning reliability method combining Kriging and Monte Carlo simulation *Struct. Saf.* **33** 145–54
[45] Huang Y, Zhang J G, Wang B W, Song L K, Wei Y X and Zhang W 2025 Active learning Kriging approach for

creep-fatigue reliability assessment of turbine disk *Structural and Multidisciplinary Optimization* p 68
[46] Shen X, Feng K, Xu H, Wang G, Zhang Y and Dai Y 2023 Reliability analysis of bending fatigue life of hydraulic pipeline *Reliab. Eng. Syst. Saf.* **231** 109019
[47] Wang X, Shi Q, Fan W, Wang R and Wang L 2019 Comparison of the reliability-based and safety factor methods for structural design *Appl. Math. Modell.* **72** 68–84
[48] Zhu T L 1993 A reliability-based safety factor for aircraft composite structures *Comput. Struct.* **48** 745–8
[49] Kachanov L M 1999 Rupture time under creep conditions *Int. J. Fract.* **97** 11–18
[50] Rabotnov Y N 1968 A model of an elastic-plastic medium with delayed yield *J. Appl. Mech. Tech. Phys.* **9** 265–9
[51] Ainsworth R 2006 R5 procedures for assessing structural integrity of components under creep and creep–fatigue conditions *Int. Mater. Rev.* **51** 107–26
[52] Wang R Z, Zhang X C, Gong J G, Zhu X M, Tu S T and Zhang C C 2017 Creep-fatigue life prediction and interaction diagram in nickel-based GH4169 superalloy at 650 °C based on cycle-by-cycle concept *Int. J. Fatigue* **97** 114–23
[53] Kwak S G and Kim J H 2017 Central limit theorem: the cornerstone of modern statistics *Korean J. Anesthesiol.* **70** 144–56
[54] Gu H H, Wang R Z, Kun Z, Wang J, Sun L, Li K S, Liu Y, Zhang X-C and Tu S-T 2023 System-level creep-fatigue reliability evaluation by engineering damage mechanics incorporating cumulative damage-damage threshold interference *Int. J. Fatigue* **176** 107768
[55] Wang R Z, Zhang X C, Gu H H, Li K S, Wen J F, Miura H, Suzuki K and Tu S-T 2023 Oxidation-involved life prediction and damage assessment under generalized creep-fatigue loading conditions based on engineering damage mechanics *J. Mater. Res. Technol.* **23** 114–30
[56] Gu H H, Wang R Z, Zhu S P, Wang X W, Wang D M, Zhang G D, Fan Z-C, Zhang X-C and Tu S-T 2022 Machine learning assisted probabilistic creep-fatigue damage assessment *Int. J. Fatigue* **156** 106677
[57] Rasmussen C E and Nickisch H 2010 Gaussian processes for machine learning (GPML) toolbox *J. Mach. Learn. Res.* **11** 3011–5
[58] Fang G, Pan R and Hong Y 2020 Copula-based reliability analysis of degrading systems with dependent failures *Reliab. Eng. Syst. Saf.* **193** 106618
[59] Cheng L Y, Wang R Z, Wang J, Zhu S P, Zhao P C, Miura H, Zhang X-C and Tu S-T 2021 Cycle-dependent creep-fatigue deformation and life predictions in a nickel-based superalloy at elevated temperature *Int. J. Mech. Sci.* **206** 106628
[60] Wang R Z, Guo S J, Chen H, Wen J F, Zhang X C and Tu S T 2019 Multi-axial creep-fatigue life prediction considering history-dependent damage evolution: a new numerical procedure and experimental validation *J. Mech. Phys. Solids* **131** 313–36

Hang-Hang Gu is currently a PhD candidate at the School of Mechanical and Power Engineering, East China University of Science and Technology. His research interests include damage-driven reliability assessment and life management.

Yuan-Ze Tang is currently a PhD candidate at the School of Mechanical and Power Engineering, East China University of Science and Technology. His research focuses on reliability assessment and life prediction of high-temperature components, with emphasis on data-physics hybrid modeling, uncertainty propagation, and machine learning-assisted reliability analysis for complex engineering systems.

Xin-Yu Yang is a research scientist at Institute of High Performance Computing (IHPC), Agency for Science, Technology and Research (A*STAR), Singapore, with research interests in physics foundation models and agentic AI systems for scientific discovery.

Run-Zi Wang is currently an Assistant Professor at the Advanced Institute for Materials Research (WPI-AIMR), Tohoku University, Japan. His research spans from modelling-driven material strength analysis to informatics-reinforced structural integrity assessment.

Professor Xian-Cheng Zhang is currently the dean of School of Mechanical and Power Engineering, East China University of Science and Technology. He is devoted to the fundamental research and technical assistance to guarantee the long-term and reliable operation of high-temperature components.